# HIGH ENERGY COSMIC RAY AIR SHOWERS AND SMALL-$X$ QCD

H.J. DRESCHER, A. DUMITRU

*Institut für Theoretische Physik*
*Johann Wolfgang Goethe-Universität*
*Postfach 11 19 32*
*60054 Frankfurt, Germany*

M. STRIKMAN

*Department of Physics*
*Pennsylvania State University*
*University Park, PA 16802, USA*

We discuss that hadron-induced atmospheric air showers from ultra-high energy cosmic rays are sensitive to QCD interactions at very small momentum fractions $x$ where nonlinear effects should become important. The leading partons from the projectile acquire large random transverse momenta as they pass through the strong field of the target nucleus, which breaks up their coherence. This leads to a steeper $x_F$-distribution of leading hadrons as compared to low energy collisions, which in turn reduces the position of the shower maximum $X_{\max}$. We argue that high-energy hadronic interaction models should account for this effect, caused by the approach to the black-body limit, which may shift fits of the composition of the cosmic ray spectrum near the GZK cutoff towards lighter elements. We further show that present data on $X_{\max}(E)$ exclude that the rapid $\sim 1/x^{0.3}$ growth of the saturation boundary (which is compatible with RHIC and HERA data) persists up to GZK cutoff energies. Measurements of $pA$ collisions at LHC could further test the small-$x$ regime and advance our understanding of high density QCD significantly.

## 1. Introduction

Today, quite little is known about the origin, the spectrum and the composition of the highest energy cosmic rays. For example, AGASA[1] found about 10 events with $E > 10^{11}$ GeV, well above the Greisen-Zatsepin-Kuzmin (GZK) cutoff, $E_{\mathrm{GZK}} \simeq 6 \cdot 10^{10}$ GeV, which arises because of interaction of protons with the cosmic microwave background. On the other hand, the results of the HIRES[2] collaboration agree with the existence of the

2

GZK cutoff (assuming isotropic sources). Forthcoming Auger[3] data near the GZK cutoff will provide higher statistics and hopefully help to resolve this puzzle.

The precise knowledge of the primary cosmic ray properties, that is the particle type, energy and arrival direction, is crucial for the interpretation of their possible source and acceleration mechanism. Standard candidates for the highest energy cosmic rays are protons or heavier nuclei, being accelerated in extreme astrophysical phenomena, or photons, arising for example from the decay of ultra-heavy $X-$particles.

Experiments detect cosmic rays indirectly via air showers induced when they enter the atmosphere. One tries to deduce the properties of the primary particle from those of the induced shower. Therefore, a good understanding of the physics of high-energy interactions in the atmosphere is mandatory. However, the maximum energies exceed those of terrestrial accelerators by far, and so our knowledge of hadronic interactions needs to be extrapolated to unknown regimes. Also, as will be discussed in more detail below, air showers are mostly sensitive to forward particle production which is less well measured in accelerator experiments.

Several features of strong interactions are expected to change dramatically at very high energies. First, the parameters of the soft interactions change - the total cross section changes by a factor of $\sim 3$, while average impact parameters increase by $\sim 50\%$. The changes in the (semi-)hard interactions are even more dramatic. Indeed, a leading parton from the projectile propagates through the very strong gluon fields in the target. For example, for a "low-energy" $p + A$ collision with $E_{\mathrm{Lab}} = 400$ GeV, a parton from the projectile carrying a momentum fraction $x_p \sim 0.1$ receiving a transverse kick of $p_t \sim 2$ GeV interacts with a gluon with $x_A = 4p_\perp^2/x_p s \sim 0.1$. At GZK energy, $E_{\mathrm{Lab}} \sim 10^{11}$ GeV, this corresponds to $x_A \sim 10^{-10}$ while *direct measurements* at HERA covered only the range $x \geq 10^{-3}$ and even indirect ones are sensitive only down to $x \geq 10^{-4}$. This is *six orders of magnitude above the x-range to which cosmic rays near the cutoff are sensitive.*

Studies at HERA indicate that the gluon density of the nucleon, $xg_N(x,Q^2)$, grows very strongly with decreasing momentum fraction $x$, roughly as $x^{-\lambda(Q^2)}$, with $\lambda(Q^2) \geq 0.2$ for $Q^2 \geq 2$ GeV$^2$. The data can be fitted by the NLO QCD evolution equations. The analysis of partial waves for the interaction of a small dipole with the nucleon at HERA energies indicates that for $q\bar{q}$ dipoles the partial waves remain substantially below the unitarity limit, while for $gg$ dipoles the unitarity limit is practically reached for virtualities $Q^2 \simeq 4$ GeV$^2$ at top HERA energies. This indicates

that for higher energies further growth of the gluon density in the proton should be tamed for a range of virtualities that increases with energy.

The rate at which the growth of the gluon density is "tamed", depends strongly on its behavior at small $x$. One of the most popular approaches for a long time was the BFKL approximation where one sums the series of leading, next to leading $\log(1/x)$. The series was found to converge poorly, to a large extent due to the specifics of the treatment of the energy conservation effects. More recent calculations[4,5] (some of which were discussed at the Erice meeting) try to treat simultaneously logarithms of both $1/x$ and $Q^2$ and to treat more accurately the phase space available for gluon emission at a given energy. They appear to indicate that the NLO DGLAP approximation should effectively work for $x \geq 10^{-3}$ for the scattering off a gluon or, correspondingly, for $x \geq 10^{-4}$ for the scattering off a nucleon, which is consistent with the HERA findings.

It appears natural to expect that the taming effects would still allow the interactions to reach the maximal possible strength allowed by unitarity over a wide range of impact parameters which should increase with energy. Indeed, this is implemented in all models currently on the market with the only difference being the rate of the approach to the unitarity limit.

If the energies are large enough, the constituents of the projectile hadron/photon propagating through the nucleus resolve strong small-$x$ gluon fields in the target. During the propagation through such media they should experience strong distortions - at the very least they should obtain significant transverse momenta inversely proportional to the size of test dipoles for which the interaction becomes black. Also, some of the processes relevant in this case, like hard scattering of the projectile partons off small-$x$ partons, lead to fractional energy losses.

However the most important effect for the purposes of near-GZK inelastic collisions is loss of coherence of the leading partons of the projectile as they acquire random transverse momenta. This leads to independent fragmentation of the leading partons from the projectile over a large range of rapidities, and hence to a much softer energy spectrum of the leading particles[6,7].

In this paper we review our first efforts to model this effect and to show its relevance for the understanding of air showers induced by cosmic rays near the GZK cutoff. Our primary goal is to analyze the implication of various models for the small-$x$ behavior of the gluon densities beyond the HERA range. We demonstrate that already the current data on the longitudinal and lateral structure of giant air showers allow us to rule out

4

certain models where gluon densities increase very rapidly with energy[8]. At the same time, models which appear to be consistent with the recent theoretical studies[4,5] lead to relatively small effects which are consistent with the air shower data and suggest that the spectrum near the cutoff is dominated by protons.

Finally, we also point out that the gluon densities encountered in central proton-nucleus collisions at LHC are similar to those for central proton-air collisions near the cutoff energy. Hence, we also present some predictions for p-"heavy nucleus" central collisions at RHIC and LHC energies which could test our suggestion for the mechanism of energy degradation by projectile breakup. Such measurements could help us understand the interactions of very high energy cosmic rays with the atmosphere and, consequently, of their composition and origin.

## 2. Scattering at high energies

The wave function of a hadron (or nucleus) boosted to large rapidity exhibits a large number of gluons at small $x$. The density of gluons per unit of transverse area and of rapidity at saturation is denoted by $Q_s^2$, the so-called saturation momentum. This provides an intrinsic momentum scale which grows with atomic number (for nuclei) and with rapidity, due to continued gluon radiation as phase space grows. For sufficiently high energies and/or large nuclei, $Q_s$ can grow much larger than $\Lambda_{\mathrm{QCD}}$ and so weak coupling methods are applicable. Nevertheless, the well known leading-twist pQCD can not be used when the gluon density is large; rather, scattering amplitudes have to be resummed to all orders in the density. When probed at a scale below $Q_s$, scattering cross sections approach the geometrical size of the hadron (the "black body" limit). A perturbative QCD based mechanism for unitarization of cross sections is provided by gluon saturation effects [9,10,11]. On the other hand, for $Q^2 \gg Q_s^2$ the process occurs in the dilute DGLAP [12] regime where cross sections are approximately determined by the known leading-twist pQCD expressions.

In this section we discuss particle production in the collision of a hadron, which for the present purposes is either a nucleon or a meson, with a target nucleus in the atmosphere. The development of the air shower is sensitive mainly to the distribution of the most energetic particles (see section 4) while the low-energy particles produced near the nuclear fragmentation region are less important for the observables studied here. Due to QCD evolution (section 2.3) this so-called forward region probes the high gluon

density (small-$x$) regime of the target, while the density of the projectile is rather low. Hence, in the relevant rapidity (or Feynman-$x_F$) region we are dealing with a "dilute" projectile hadron impinging on a "dense" target nucleus: $Q_s^h < Q_s^A$.

This assumption breaks down at large impact parameters, where even the saturation momentum of the nucleus, $Q_s^A(y, b)$, is not large. For such events, as well as for collisions at moderately high energies, no intrinsic semi-hard scale exists in the problem and so a treatment within weak coupling QCD is not applicable. In accelerator experiments this regime could be avoided by appropriately tuning the control parameters, such as collision energy, atomic number of projectile and target, impact parameter (trigger), rapidity $y$, transverse momentum $p_t$ and so on. This, of course, is not feasible in the case of cosmic ray air showers; here, we model such collisions using the SIBYLL leading-twist event generator. This is discussed in more detail in section 3.

### 2.1. *Leading quarks*

With this in mind, we now focus on particle production in collisions at sufficiently high energy and sufficiently small impact parameter where the saturation momentum of the nucleus is large enough to warrant a weak-coupling approach. The dominant process for fast particle production ($x_F \gtrsim 0.1$) is scattering of quarks from the incident dilute projectile on the dense target. For high quark energy we assume that the eikonal approximation applies such that $p^+$ is conserved. The transverse momentum distribution of scattered quarks is then given by the correlation function of two Wilson lines,

$$V(x_t) = \hat{P} \exp\left[ -ig \int_{-\infty}^{\infty} dz^- A^+(z^-, x_t) \right] \;, \tag{1}$$

running up and down the light cone at transverse separation $r_t$ (in the amplitude and its complex conjugate),

$$\sigma^{qA} = \int \frac{d^2 q_t dq^+}{(2\pi)^2} \delta(q^+ - p^+) \left\langle \frac{1}{N_c} \operatorname{tr} \left| \int d^2 z_t \, e^{i\vec{q}_t \cdot \vec{z}_t} \left[ V(z_t) - 1 \right] \right|^2 \right\rangle \;. \tag{2}$$

Here, the convention is that the incident hadron has positive rapidity, i.e. the large component of its light-cone momentum is $P^+$, and that of the incoming quark is $p^+ = xP^+$ ($q^+$ for the outgoing quark). The two-point function has to be evaluated in the background field of the target nucleus. When this field is weak, the Wilson lines can be expanded to leading order

6

and the problem reduces to evaluating the two-point function of the gauge field $A^\mu$.

In the strong-field regime $gA^+ \sim 1$, however, one needs to evaluate the correlation function to all orders (corresponding to summing over any number of scatterings of the incident quark). A relatively simple closed expression can be obtained in the McLerran-Venugopalan model of the small-$x$ gluon distribution of the dense target[10]. In that model, the small-$x$ gluons are described as a stochastic classical non-abelian Yang-Mills field which is averaged over with a Gaussian distribution. $n$-point functions then factorize into powers of the two-point function. The $qA$ cross section is then given by[13]

$$q^+ \frac{d\sigma^{qA \to qX}}{dq^+ d^2 q_t d^2 b} = \frac{q^+}{P^+} \delta \left( \frac{p^+ - q^+}{P^+} \right) C(q_t) \tag{3}$$

$$C(q_t) = \int \frac{d^2 r_t}{(2\pi)^2} e^{i\vec{q}_t \cdot \vec{r}_t} \left\{ \exp \left[ -2Q_s^2 \int_\Lambda \frac{d^2 l_t}{(2\pi)^2} \frac{1}{l_t^4} \left( 1 - e^{i\vec{l}_t \cdot \vec{r}_t} \right) \right] \right.$$
$$\left. - 2 \exp \left[ -Q_s^2 \int_\Lambda \frac{d^2 l_t}{(2\pi)^2} \frac{1}{l_t^4} \right] + 1 \right\} . \tag{4}$$

This expression is valid to leading order in $\alpha_s$ (tree level), but to all orders in $Q_s$ since it resums any number of scatterings of the quark in the strong field of the nucleus. The saturation momentum $Q_s$, as introduced in eq. (3), is related to $\chi$, the total color charge density squared (per unit area) from the nucleus integrated up to the rapidity $y$ of the probe (i.e. the projectile quark), by $Q_s^2 = 4\pi^2 \alpha_s^2 \, \chi \, (N_c^2 - 1)/N_c$. In the low-density limit, $\chi$ is proportional to the ordinary leading-twist gluon distribution function of the nucleus[14]:

$$\chi(x) = \frac{A}{\pi R_A^2} \int_x^1 dx' \left( \frac{1}{2N_c} \, q(x', Q_s^2) + \frac{N_c}{N_c^2 - 1} \, g(x', Q_s^2) \right) , \tag{5}$$

where $q(x)$ and $g(x)$ denote the quark and gluon distributions of a nucleon, respectively; note that shadowing in the linear regime[15] would tend to reduce $\chi$ somewhat but is neglected here since we are dealing with small nuclei (mass number $14 \to 16$) and because the induced air showers are sensitive mainly to the small-$x$ regime in the nucleus.

The integrals over $p_t$ in eq. (3) are cut off in the infrared by some cutoff $\Lambda$, which we assume is of order $\Lambda_{\rm QCD}$. At large transverse momentum, again the first exponential in (3) can be expanded order by order[16,17] to generate the usual power series in $1/q_t^2$:

$$C(q_t) = \frac{1}{2\pi^2} \frac{Q_s^2}{q_t^4} \left[ 1 + \frac{4}{\pi} \frac{Q_s^2}{q_t^2} \log \frac{q_t}{\Lambda} + O\left( \frac{Q_s^2}{q_t^2} \right) \right] . \tag{6}$$

This expression is valid to leading logarithmic accuracy. The first term corresponds to the perturbative one-gluon $t$-channel exchange contribution to $qg \to qg$ scattering and exhibits the well-known power-law divergence of leading-twist perturbation theory for small momentum transfer.

On the other hand, for $Q_s \gtrsim q_t$ one obtains in the leading logarithmic approximation[17]

$$C(q_t) \simeq \frac{1}{Q_s^2 \log Q_s/\Lambda} \, \exp\left(-\frac{\pi q_t^2}{Q_s^2 \log Q_s/\Lambda}\right) \; . \tag{7}$$

This approximation reproduces the behavior of the full expression (3) about $q_t \sim Q_s$, and hence the transverse momentum integrated cross section reasonably well. It is useful when the cutoff $\Lambda \ll Q_s$, that is, when color neutrality is enforced on distance scales of order $1/\Lambda \gg 1/Q_s$. If, however, color neutrality in the target nucleus occurs over distances of order $1/Q_s$[18] then $\Lambda \sim Q_s$ and one has to go beyond the leading-logarithmic approximation.

It is essential to realize that the high-energy part of the air shower is essentially one-dimensional, i.e. the transverse momenta of the produced *hadrons* play no role[a] (see section 4). This, in turn, implies that when $Q_s$ is large that the high-transverse momentum leading-twist regime can be neglected. The $q_t$-distribution of forward valence quarks can thus be taken to be given by the simple expression (7) rather than (4). Note also that both expressions do conserve probability, i.e.

$$\int d^2q_t \, C(q_t) = 1 \; . \tag{8}$$

This is, of course, a very useful property because all charges carried by the valence quarks are then automatically conserved.

Contrary to the leading twist expression (6), the distribution (7) exhibits transverse broadening as the density of the target increases (the scattered quarks are pushed out to larger $q_t$). Consider now the probability of inelastic scattering (i.e. *with* color exchange) to small transverse momentum. This is given by expression (4,7), integrated from $q_t = 0$ to $q_t = \Lambda$:

$$\int_0^\Lambda d^2q_t \, C(q_t) \simeq \frac{\pi \Lambda^2}{Q_s^2 \log Q_s/\Lambda} + \cdots \; . \tag{9}$$

---

[a]We repeat, however, that the transverse broadening of the distributions of released *partons does* play an important role since it destroys the coherence of the projectile wave function[7] and affects the fragmentation into hadrons.

8

Here, we have written only the leading term in $\Lambda^2/Q_s^2$, neglecting subleading power-corrections and exponentially suppressed contributions. Hence, soft forward inelastic scattering is power-suppressed in the black body limit because the typical transverse momentum is proportional to $Q_s^A$. This steepens the longitudinal distribution $dN/dx_F$ of leading particles since partons with large relative momenta fragment independently[6,7]. On the other hand, for low target density, the projectile's coherence is not destroyed completely and leading quarks may recombine, recovering the "leading-particle" effect observed in $pp$ scattering at not too high energy. This recombination effect should be taken into account when modeling minimum bias $pA$ collisions in order to ensure a smooth transition from the high-density to the low-density regime; our implementation is described and studied in more detail in section 3.

Integrating over the transverse momentum of the scattered quark, the elastic and total scattering cross sections for quark-nucleus scattering are[13]:

$$\sigma^{\mathrm{el}} = \int d^2b \left[ 1 - \exp(-Q_s^2/4\pi\Lambda^2) \right]^2 \tag{10}$$

$$\sigma^{\mathrm{tot}} = 2 \int d^2b \left[ 1 - \exp(-Q_s^2/4\pi\Lambda^2) \right] . \tag{11}$$

Clearly, when $Q_s/\Lambda \to \infty$, the cross section approaches the unitarity limit.

## 2.2. *Gluons*

Gluon bremsstrahlung dominates particle production at $x_F \lesssim 0.1$. At very large transverse momentum, $q_t \gg Q_s$, the inclusive gluon distribution is given in collinear factorization by the usual $gg \to gg$ LO hard scattering function convoluted with the DGLAP evolved leading-twist gluon distribution of the projectile and target. However, for the high-energy part of the air shower only the $p_t$-integrated longitudinal distribution of hadrons matters (cf. section 4) which is dominated by fragmentation of gluons with transverse momenta up to $\sim Q_s^A$. In that regime leading-twist perturbative QCD can not be applied reliably.

Gluon radiation with transverse momentum $q_t \sim Q_s^A$ in high-energy hadron-nucleus collisions has been discussed in detail in[19,20]. The release of gluons from the hadronic wave functions can be described by convoluting the gluon distribution in the hadron with a (semi-)hard scattering cross section. The main qualitative features of the bremsstrahlung spectrum is that it flattens from $\sim 1/q_t^4$ for asymptotically large $q_t$ to $1/q_t^2$ for $q_t$ in

between the two saturation momenta; for $q_t \to 0$, finally, it approaches a constant (up to logarithms)[21].

For the present purposes we require a simple *ansatz* that can be easily implemented in a Monte-Carlo model and, at the same time, does incorporate the above features. A useful approach has been suggested in refs.[20]. The "fusion" of two gluon ladders gives rise to the bremsstrahlung spectrum

$$E\frac{d\sigma}{d^3q} = 4\pi \frac{N_c}{N_c^2 - 1} \frac{1}{q_t^2} \int\limits^{q_t^2} dk_t^2 \, \alpha_s(k_t^2) \, \phi_h(x_1, k_t^2) \, \phi_A(x_2, (q_t - k_t)^2) \ , \quad (12)$$

where $\phi(x, Q^2)$ denotes the unintegrated gluon distribution function of the projectile hadron or target nucleus, respectively. It is related to the gluon density by

$$x \, g(x, Q^2) = \int\limits^{Q^2} dk_t^2 \, \phi(x, k_t^2) \ . \quad (13)$$

Eq. (12) can be integrated by parts to read

$$\frac{dN}{dy dq_t^2} = 4\pi \alpha_s(q_t^2) \, \frac{N_c}{N_c^2 - 1} \frac{1}{q_t^4} \, x_1 g_h(x_1, q_t^2) \, x_2 g_A(x_2, q_t^2) \ . \quad (14)$$

The *ansatz* from[20] for the infrared-finite gluon densities is

$$x \, g(x, Q^2) \propto \frac{1}{\alpha_s} \min(Q^2, Q_s^2(x)) \, (1 - x)^4 \ , \quad (15)$$

with $\alpha_s$ evaluated at $\max(Q_s^2, Q^2)$. Note that for large $Q^2$, the $x$-dependence of the gluon distribution exhibits the conventional $xg(x) \sim x^{-\lambda}(1 - x)^4$ behavior; this follows from the evolution of the saturation momentum[b] $Q_s(x) \sim 1/x^\lambda$ with $x$. On the other hand, for small $Q^2$ and $x$, the above *ansatz* exhibits a slow logarithmic growth $xg(x) \sim \log \, x^{-\lambda}$ only. In any case, we consider (15) to be a simple parameterization which exhibits some generic qualitative features expected from gluon saturation (e.g. that it is of order $1/\alpha_s$ at small $Q^2$ and $x$) while, at the same time, it is roughly consistent with the DGLAP gluon distribution at large $Q^2$ and $x$. In fig. 1 we compare the parameterization (15), with the normalization constant fixed by the condition $\int dx \, xg(x, Q^2) = 0.5$ and with $Q_s^2 \sim x^{-0.3}$, to the CTEQ5 LO distribution[22].

---

[b]For fixed coupling evolution this is true for any $x$; for running coupling evolution it holds only for not too small $x$, see section 2.3.
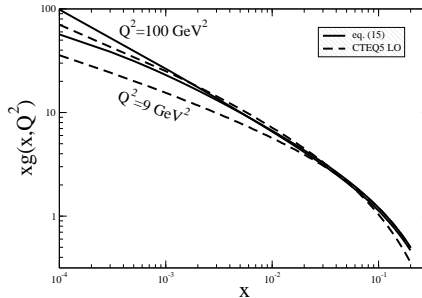
10



Figure 1.   Comparison of the gluon distribution from eq. (15) with CTEQ5 LO, in the DGLAP regime (for a proton).

The constant of proportionality in eq. (15) was chosen in[20] such as to reproduce the overall normalization of the charged hadron rapidity distribution in $d+Au$ collisions at BNL-RHIC energy. This was possible because the forward region was not considered. On the other hand, here we need to consider the entire solid angle (in momentum space) and, in particular, ensure conservation of the energy carried by the projectile. In our approach we therefore fix the overall number of radiated gluons by the condition of energy conservation. This is discussed in more detail in section 3 where we also show that the charged hadron multiplicity in the central region of $pA$ collisions at BNL-RHIC energy agrees roughly with that from[20] and with available data.

### 2.3.  *The saturation momentum as a function of impact parameter and rapidity*

The saturation momentum of the nucleus, $Q_s^A$, must of course depend on the impact parameter as it basically measures the color charge density in the transverse plane. Hence, in the rest frame of the nucleus, the most naive estimate (neglecting shadowing[15]) is that there are $A$ times more valence quarks in a nucleus than in a nucleon which are distributed over an area proportional to $A^{2/3}$; this then results in $(Q_s^A)^2 \sim A^{1/3}$. More elaborate estimates lead to an additional factor equal to the logarithm of the mass number.

For realistic nuclei with a non-uniform density distribution in the transverse plane we must replace, of course, the $A^{1/3}$ factor by the number of nucleons from the target which interact with the projectile, $N_A$:

$$N_A(b) = A\sigma_{\rm in}(s)T_A(b) \tag{16}$$

with $T_A(b)$ the nuclear profile function[c] and $\sigma_{in}(s)$ the energy dependent inelastic (non single-diffractive) cross section for the particular projectile species on protons. Fluctuations in $N_A(b)$ are also taken into account in our Monte-Carlo implementation, as discussed in section 3. The impact parameter dependence of the nuclear saturation momentum is then taken to be

$$Q_s^A(b) = \Lambda\sqrt{[1 + N_A(b)]\ \log(1 + N_A(b))}\ . \qquad (17)$$

For a single nucleon, this corresponds to a saturation momentum on the order of $\Lambda$. It should be noted that at very high energies, deep in the black-body limit, the results depend only weakly on the above "initial condition" for $Q_s^A$. However, when the saturation momentum is only moderately large (for example, for running coupling evolution, see below), the assumed dependence of $Q_s^A$ on $b$ could play a role. Whether or not $Q_s^2 \sim N_A$ is the most appropriate choice will be studied in more detail in the future.

Next, we turn to the dependence of $Q_s$ on rapidity[d] $y = \log 1/x$. Eq. (17) provides the initial condition in (or near) the rest frame of the nucleus, $y \simeq 0$, from valence quarks. As one moves away in rapidity phase space for gluon radiation opens up and so the gluon density grows; it is expected to saturate when it becomes of order $1/\alpha_s$ [11]. For a recent review of evolution at small $x$ see e.g.[23].

Model studies of deep inelastic scattering (DIS) on protons at HERA suggest[24]

$$Q_s^2(x) \sim x^{-\lambda} \qquad (18)$$

with $\lambda \approx 0.3$. This scaling relation can be obtained from the *fixed coupling* BFKL evolution equation for the scattering amplitude of a small dipole. The BFKL equation is a linear QCD evolution equation which can not be applied in the high-density regime. Nevertheless, one can evolve the wave function of the target in rapidity $y = \log 1/x$ and ask when the dipole scattering amplitude becomes of order one, which leads to[e]

$$Q_s^2(y, b) = Q_s^2(y_0, b)\exp c\bar{\alpha}_s y\ , \qquad (19)$$

with $\bar{\alpha}_s = \alpha_s N_c/\pi$ and $c \approx 4.84$ a constant. Hence, LO fixed-coupling BFKL evolution predicts $\lambda' = c\bar{\alpha}_s$ of order one, a few times larger than the

---

[c]Normalized according to $\int d^2 b T_A(b) = 1$.

[d]In this section, we measure the rapidity always relative to the parent hadron.

[e]We write only the leading term proportional to $y$.

12

fit (18) to HERA phenomenology. A resummed NLO BFKL analysis corrects this discrepancy and leads to $\lambda'$ much closer to the phenomenological value[25]. A similar observation is made in[5] where both $\log(1/x)$ and $\log Q$ effects were considered.

On the other hand one could also consider BFKL evolution with ad-hoc one-loop running of the coupling[23f]: $\bar{\alpha}_s(Q_s^2) = b_0/\log(Q_s^2(x)/\Lambda_{\rm QCD}^2)$, which leads to

$$Q_s^2(y,b) = \Lambda_{\rm QCD}^2 \exp \sqrt{2b_0 c(y+y_0)} \; , \tag{20}$$

with $2b_0 c y_0 = \log^2(Q_0(b)^2/\Lambda_{\rm QCD}^2)$. Insisting that (18) be valid at least in the $y \to 0$ limit again provides us with a phenomenological value for the constant $c$ in terms of the saturation momentum at $y = 0$. The form (20) leads to a notably slower growth of $Q_s$ at high energy. Specifically, for central proton-nitrogen collisions at RHIC, LHC and GZK-cutoff energies (total rapidity $y = 10.7$, 17.3 and 26.0) the saturation momentum of the nucleus in the rest frame of the projectile hadron is $Q_s = 1.5$, 5, 20 GeV for fixed coupling evolution, while for running coupling evolution it is $Q_s = 1$, 2.5, 6 GeV, respectively. Clearly, cosmic ray interactions in our atmosphere should offer a realistic opportunity for distinguishing these scenarios.

### 3. Monte-Carlo implementation

We first generate a configuration of valence quarks according to the distribution (3,7), convoluted with the respective valence quark distribution of the projectile at the scale $Q_s^A$ [7]:

$$\frac{d\sigma}{dx d^2 q_t d^2 b} = f_{\rm v}(x, Q_s^A) \, C(q_t) \tag{21}$$

with $Q_s^A$ is a function of both $x$ and $b$. For this purpose, we employ the GRV94 parameterization of the parton distribution functions of a proton[26] or a $\pi^+$[27]; we assume isospin symmetry to deduce the distributions for other states. Also, as a rough approximation we take the valence quark distribution of the $K^+$ to be the same as that of the $\pi^+$, with the replacement $\bar{d} \to \bar{s}$.

The remaining momentum is then used to generate a number of gluons according to the distribution (14). These gluons could be fragmented independently but this is not a good approximation when their transverse

---

[f] Again, we drop subleading terms that grow more slowly with rapidity.

momenta are soft. Rather, soft collinear gluons should be absorbed by the parent parton.

The Lund string model[28] provides such an infrared safe fragmentation prescription. We order the produced gluons in rapidity and place them on strings between the valence quarks and the target nucleus, whose precise configuration is not important. (Target fragmentation produces only low-energy particles which do not affect the properties of the air shower discussed here.)

A baryon-nucleus collision produces three strings (two for a meson-nucleus collision). However, when the invariant mass of any two of the three valence quarks is small, one cannot assume anymore that those strings fragment independently. Rather, they will recombine to form a leading diquark, recovering the "leading particle effect" for low $Q_s^A$. This effect should be taken into account in order to ensure a smooth transition from the regime of high target density (high energy, central collisions) to low target density (lower energy, large impact parameter). We model this by introducing a cut-off in invariant mass,

$$m_{\mathrm{cut}} = m_\rho = 0.77 \text{ GeV} \tag{22}$$

below which two leading quarks are allowed to form a diquark. The effect on the $x_F$-distribution of fast hadrons is shown below.

Although soft gluon absorption and diquark recombination are taken into account in our Monte-Carlo implementation of scattering near the black body limit of QCD ("BBL"), it should nevertheless be clear that it is restricted to the high-density regime. For example, when $Q_s^A$ becomes small, the DGLAP leading-twist regime becomes important and one should use better approximations for the gluon densities than those from (15). Also, the fraction of diffractive and elastic events becomes sizable.

A large amount of work has been done to develop models for this regime. SIBYLL[29] and QGSJET[30], in particular, are commonly used to model air showers. We do not intend to duplicate those approaches here but rather to study whether anything could be learned about small-$x$ QCD from cosmic ray air showers. Hence, we couple our model to the standard pQCD leading twist event generator SIBYLL 2.1 such that the "BBL" Monte-Carlo treats the high density regime (large saturation momentum of the nucleus, i.e. high energy and/or small impact parameter) while SIBYLL handles peripheral or low energy collisions where the saturation momentum of the nucleus is not sufficiently large.

It is clear, of course, that no sharp boundary between those regimes

14

exists and that this artificial separation is performed for purely technical reasons. It is therefore important to check that the results do not depend strongly on the precise location of the assumed boundary between low and high density. As already mentioned above, we do implement some effects into the BBL model which should facilitate a smooth transition to low densities, such as soft gluon absorption and diquark recombination. At the same time, the SIBYLL model also assists the transition to high target densities by implementing a low-$p_t$ cutoff for the DGLAP regime which grows rapidly with energy, see Engel et al[29]. We therefore expect that our results are not very sensitive to where exactly we perform the switch, as long as it occurs in a reasonable regime; this will be checked below.

The saturation momentum of the nucleus provides an intrinsic scale for resolving the valence quark structure of the projectile, cf. eq. (21). In practice, this scale can not be too small because the $Q^2$ evolution of parton distributions in hadrons is normally obtained from DGLAP; standard PDF parameterizations typically require a minimal $Q^2$ on the order of $1$ GeV$^2$. In order not to distort the inclusive momentum distribution of valence quarks, we must therefore ensure that $Q_s^A(x)$ does not drop below this threshold at too large an $x$. Specifically, we require that the valence quark distribution be probed at least down to $x = 10^{-3}$:

$$Q_s^A(x = 10^{-3}, b) > Q_{\min} \approx 1 \text{ GeV} . \qquad (23)$$

In our Monte-Carlo approach, the collision is handled by either BBL or SIBYLL depending on whether this condition is met or not. The resulting boundary between low and high density regimes appears reasonable; for example, for central collisions of protons on heavy targets like $Au$ or $Pb$, the transition occurs just below BNL-RHIC energy, $\sqrt{s} = 200$ GeV. On the other hand, minimum bias $pp$ collisions essentially never pass the threshold (23), even at LHC energies and beyond.

As a first check, we apply our model to RHIC energy which represents the highest presently available energy for proton-nucleus collisions. We compare the (pseudo-) rapidity distribution of inclusive charged hadrons to data by BRAHMS[31]. The fragmentation region of the target should be disregarded since no attempt has been made to treat that realistically. Given that no special tuning has been performed to fit these particular data[g], we consider the qualitative agreement to be quite good. More importantly, we

---

[g]For example regarding diquark recombination, string fragmentation or initial conditions for the evolution of the two saturation momenta
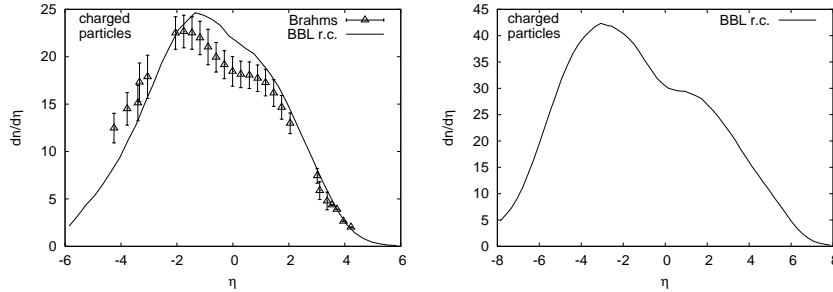
Figure 2.   Left: Comparison of the BBL event generator (with running coupling evolution) to RHIC data ($E_{\mathrm{CM}} = 100$ GeV) from $d + Au$ collisions by the BRAHMS collaboration [31]. We have scaled our results for $p + Au$ (obtained with $N_A = 6$ participants) by a factor of two. Right: our prediction for central $p + Pb$ collisions at LHC energy, (assuming $N_A = 10$ and $E_{\mathrm{CM}} = 3000$ GeV).

note that both evolution scenarios (running and fixed coupling) can easily be made to fit the same data at this energy by somewhat readjusting the initial conditions for $Q_s$ (see for example[20] for a much better fit than ours with fixed-coupling evolution). Hence, RHIC energy is too low to reliably probe the evolution of $Q_s$; rather, results are mostly sensitive to the initial conditions.

In the right panel we show our result for central $p + Pb$ collisions at LHC energy, which roughly agrees with that from ref.[32]. Note, however, that ref.[32] considers the overall normalization to be a parameter, fixed from low-energy (RHIC) collisions, while in our approach it is determined automatically by momentum conservation. The similarity of $dN/d\eta$ at central rapidities obtained via the two methods perhaps suggests that indeed the number of radiated gluons equals the maximum number allowed by kinematics.

Figure 3 shows the $x_F$ distribution of pions and nucleons for central proton-nitrogen events at $10^9$ GeV. We plot on a logarithmic scale to show the effect at high $x_F$. Very forward particle production is suppressed as compared to the pQCD model SIBYLL 2.1, which is a consequence of the break-up of the projectile into its partonic components. This behavior affects another key quantity for cosmic ray air showers, the so-called inelasticity, which is one minus the Feynman-$x$ of the most energetic secondary hadron (shown below). Also note that in the high-density limit diquark recombination in the forward region is suppressed (see discussion below), and so the projectile proton mainly decays into a beam of leading mesons[7].
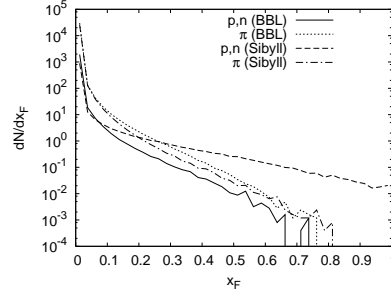
16



Figure 3.   Comparison of the SIBYLL 2.1 and BBL models for central $p +^{14}N$ events at $E = 10^9$ GeV. For either model, we show the nucleon and pion spectra separately. One observes the suppression of forward nucleon production in the high-density limit, which is due to the complete breakup of the proton.

It would be very useful to check this prediction in central $p + Pb$ collisions at the LHC in order to confirm or rule out the basic mechanism of energy degradation presented here, which is very important for cosmic ray air showers.
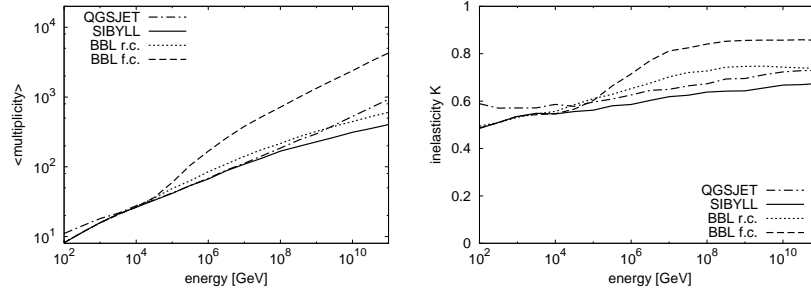


Figure 4.   Mean multiplicity of charged particles (left panel) and the inelasticity (right panel) as a function of lab energy, for minimum bias $p +^{14}N$ collisions.

Fig. 4 compares the mean multiplicities of charged particles from the BBL model with fixed and running coupling evolution of the saturation scale, and the conventional models SIBYLL 2.1 and QGSJET01. Most significant is the difference between fixed and running coupling evolution. For fixed coupling evolution $Q_s^A$ grows very large over a broad range of impact parameters (the radius of the black disc approaches the geometrical cross section of the target nucleus). Hence, even for minimum bias collisions

forward particle production is strongly suppressed in this case, and the re-maining energy is used for particle production at small $x_F$. This explains the large multiplicities as compared to BBL with running coupling evolu-tion. On the other hand, for energies below $10^4 - 10^5$ GeV there is little sensitivity to the evolution scenario for $Q_s^A$ and the results look rather sim-ilar. In SIBYLL 2.1, the growth of the multiplicity is "tamed" by a rapidly growing $p_t$-cutoff for leading-twist hard processes. It should be kept in mind though that the multiplicity from large momentum transfer processes is power-law sensitive to the infrared cutoff.
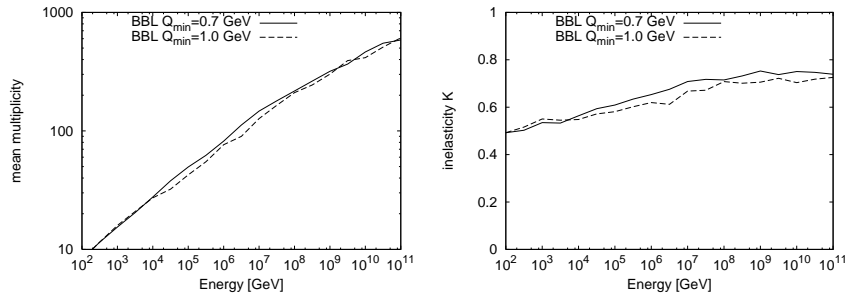


Figure 5.    The mean charged particle multiplicity and the inelasticity for minimum-bias $p +^{14}N$ collisions using the combined BBL+SIBYLL 2.1  model for $Q_{\min} = 0.7,\ 1.0$ GeV.

To check the sensitivity to the (artificial) boundary between low and high density from eq. (23), we compare results for the multiplicity and for the inelasticity for $Q_{\min} = 0.7$ GeV and $Q_{\min} = 1$ GeV in Fig. 5. A lower value for $Q_{\min}$ leads to a higher fraction of BBL events, but these are then generated with lower $Q_s^A$, and so are more similar to "soft" events from SIBYLL. In total, we see that there is little sensitivity of physical observables to the precise threshold between the models, as long as it is chosen within reasonable bounds. In the following we chose $Q_{\min} = 0.7$ GeV as default for our calculations.

In Fig. 6, finally, we show the effect of the diquark recombination mech-anism. We compare the production of protons and neutrons in central colli-sions to the case without recombination ($m_{\mathrm{cut}} = 0$). At relatively low ener-gies ($E \approx 10^6$ GeV), one notices a suppression of forward baryon production when recombination is not taken into account, except for $x_F \approx 1$. This very forward peak is in fact produced by elastic or diffractive events within the SIBYLL model, which still handles about 5% of all central collisions at this
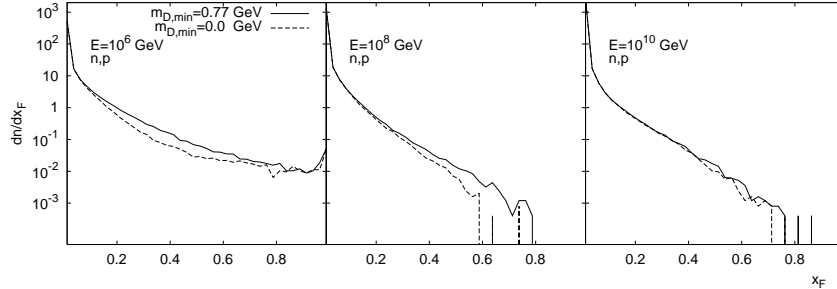
18



Figure 6.    Diquark recombination effect for $p + {}^{14}N$ collisions at various energies.

energy if $Q_s$ obeys running coupling evolution[h]. At $E = 10^8$ GeV and above, essentially all central collisions occur near the black body limit, i.e. they pass criterion (23). The diquark recombination mechanism then allows more particles to be produced in the forward region since the momenta of the corresponding valence quarks are combined. Nevertheless, the effect is less important at higher energies since there $Q_s^A$ is already too high to allow for the production of a diquark system with low invariant mass.

## 4.  Air showers

In section 4.1 we give a brief introduction into concepts and observables in cosmic ray physics for readers from other fields. More detailed discussions can be found in dedicated textbooks such as the book by Gaisser[33].

In section 4.2 we discuss general aspects of air shower simulation and, in particular, present the so-called cascade equations[34] employed here to solve for the longitudinal shower profile. From those equations, we can cleanly identify which "input" is required from QCD for their solution and, indeed, which properties of high-energy hadronic interactions actually influence the characteristics of very high energy air showers.

### 4.1.  *Introduction to air showers*

Due to a very low flux at high energies, cosmic rays are detected indirectly by the measurement of air showers. These are cascades of particles produced

---

[h]We note that the actual configuration of nucleons in the target is generated randomly in each event by SIBYLL according to the appropriate nuclear density profile. Hence, fluctuations in the number of target participants are taken into account.
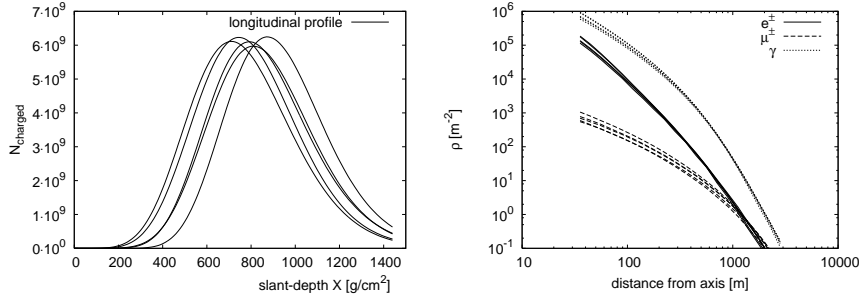
Figure 7. Longitudinal profiles and lateral distribution function of typical showers; here $E_0 = 10^{10}$ $GeV$.

by the interaction of the primary cosmic ray and subsequent secondaries with air nuclei. An air shower can be structured into 3 parts: a hadronic, an electromagnetic and a muonic part. Hadrons are produced in collisions with air-nuclei. Most of the electromagnetic part is induced by $\pi^0$-decays, which have a short life-time and decay instantly up to $10^{19}$ eV. Muons are produced by decays of charged pions and kaons, but since their decay-length is much longer only low energies particles decay while at higher energies collision with air nuclei dominates. Once produced, muons propagate with little interaction (mostly energy-loss) through the atmosphere until they decay or reach the ground. The most prominent fraction of a shower is the electromagnetic part. A rule of thumb is that the number of electrons and positrons at the maximum of the shower is approximately 60% of the primary energy $E_0$ measured in GeV (a $10^{11}$ GeV shower produces about 60 billion particles !).

There are two basic observables associated with air showers, which are measured by experiments: the longitudinal shower profile and the lateral distribution functions. The longitudinal profile is the number of charged particles measured along the shower-axis. One typically expresses this as a function of slant-depth, which is the density of the atmosphere integrated along the shower-axis: $X = \int_\infty^p \rho_{\mathrm{Air}}(l)dl$. For a vertical shower, $X$ ranges from zero (top of the atmosphere) to 1020 g/cm$^2$ (sea level). For inclined showers with polar angle up to $60°$, the slant depth is related to the vertical depth by $X = X_v/\cos(\theta)$; at larger angles one has to take into account the curvature of the earth. Typical shower profiles are shown in Fig. 7. The position where the profile reaches the maximum is defined as the shower maximum $X_{\max}$, the number of charged particles is called the shower size $N_{\max}$. For a fixed energy these values fluctuate quite substantially, which is

20

due to the fact that the depth of the first collision can vary according to the cross section. One therefore usually compares the mean $X_{\max}$ for a given primary and energy $E_0$. An important observation is that $X_{\max} \propto \log(E_0)$ and $N_{\max} \propto E_0$. To first approximation, the shower of a nucleus can be considered to be a superposition of $A$ independent nucleon-initiated showers, each carrying an energy $E_0/A$ ($E_0$ is the total energy of the primary, not per nucleon). The mean $X_{\max}^{\text{Fe}}$ of an iron-induced shower is therefore lower than that of a proton induced shower, roughly corresponding to the mean $X_{\max}$ of a proton shower at energy $E_0/A$. Experiments measure the longitudinal profile via the emitted fluorescence light of nitrogen as the shower swipes through the atmosphere. The energy of the primary cosmic ray is then proportional to the total number of charged particles, which is determined by integrating the profile.

A very important quantity for $X_{\max}$ is the inelastic cross section of a particle on air. It determines the mean free path in the atmosphere. A significant amount of uncertainty in models for the longitudinal distribution of air showers is due to this variable.

The other observable, the lateral distribution function (LDF), describes the density of particles measured on the ground as a function of the distance from the shower axis (hence in the shower plane) for given particle types[i]. Most of the lateral spread is generated by low-energy scattering of the electromagnetic part of an air shower. Hadrons do not spread out very much to large distances, only the low energy ones influence the tail of the LDF by producing $\pi^0$ at large angles or distances[j]. Typical LDFs are depicted in Fig. 7 (right panel). They follow approximately a power law. Just as $X_{\max}$, the slope of the LDF also fluctuates. Showers induced higher in the atmosphere lead to flatter LDFs since they spread out over a larger radial distance. Empirically, one finds that these fluctuations cancel at some distance from the shower axis. Experiments exploit this property to extract the primary energy of the cosmic ray, which is taken to be proportional to the density at some distance from the axis. The proportionality constant is normally computed from simulations.

When studying high energy particle physics with air showers it is important to notice that the high-energy part of the shower (i.e. the first

---

[i]Experiments measure the density in terms of response of whatever detector they use, e.g. scintillation or Cerenkov light, and normalize by the average signal of atmospheric muons, which are used for calibration.

[j]Hence, LDFs constrain mostly the *low-energy* hadronic interaction models[35].

collisions) is almost purely longitudinal, which follows from simple kine-matics. The targets (air-nuclei) are at rest and the projectiles have huge $\gamma$-factors, resulting in very small scattering angles. Furthermore, forward scattering is most important in air showers, since large-$x_F$ particles carry most of the energy. This implies, for example, that high-$p_t$ QCD jets at mid-rapidity do not influence the longitudinal shower profile substantially nor do they contribute significantly to the lateral spread (see also ref.[36]).

### 4.2. *Simulation of air showers*

The simulation of air showers is crucial for cosmic ray physics, since they are needed for the interpretation of experimental data. Given a hadronic interaction model[k], and models for electromagnetic and muonic interactions one could just follow each particle and subsequent secondaries individually. Of course, since $N \propto E_0$, this would require huge amounts of computing time at very high energies. Therefore, Hillas introduced the thinning algo-rithm: below a given energy threshold, i.e. for $E < f_{\rm th} \times E_0$, only one single secondary particle from a collision is followed, but it is attributed a higher weight. However, for a large thinning level $f_{\rm th}$, this introduces artificial fluctuations into the air shower.

On the other hand, the fact that at high energies the lateral part of the hadronic shower can be neglected suggests another efficient ap-proach to solve this problem, which is based on one-dimensional transport equations[34]:

$$\frac{\partial h_n(E,X)}{\partial X} = -h_n(E,X) \left[ \frac{1}{\lambda_n(E)} + \frac{d_n}{E\rho(X)} \right] \tag{24}$$

$$+ \sum_m \int_E^{E_{\max}} h_m(E',X) \left[ \frac{W_{mn}(E',E)}{\lambda_m(E')} + \frac{d_m D_{mn}(E',E)}{E'\rho(X)} \right] dE' \quad .$$

Here, $h_n(E,X)dE$ is the number of particles of type $n$ at altitude $X$ in the given energy range $[E, E+dE]$; the functions $W_{mn}(E',E)$ are the energy-spectra $dN/dE$ of secondary particles of type $n$ in a collision of hadron $m$ with air; $D_{mn}(E',E)$ are the corresponding decay functions; $d_n = m_n/(c\tau_n)$ is the decay constant, and $\lambda_n(E) \propto 1/\sigma_{\rm inel}$ is the mean free path of the par-ticle. The first term in (24) with the minus sign accounts for particles dis-appearing by either collisions or decays, whereas the source term accounts

---

[k]Typically a Monte-Carlo event generator which generates complete final states and accounts for fluctuations.

22

for production of secondary particles by collisions or decays of particles at higher energies. Primary particles appearing in eq. (24) are nucleons (protons, neutrons and their anti-particles), charged pions, charged and neutral kaons. In addition, we have as secondaries $\pi^0$s and photons (as direct decay products from $\eta$ mesons, for example) which feed the electromagnetic cascade and muons as decay products of charged mesons.

To summarize, the basic ingredients for constructing longitudinal profiles of air showers are the inclusive spectra $dN_n/dx_F$ of the non-strongly decaying particles and their inelastic cross sections, which determine the mean free path. The electromagnetic cascade can be treated in a similar way[37].

The first few interactions in an air shower are the main source of fluctuations in $X_{\max}$ (and, accordingly, in the LDF). Since the cascade equations cannot account for those (they solve for a mean shower) one could treat the high energy part by a traditional Monte-Carlo method. This is the so-called hybrid approach to air shower simulations. On the other hand, if one solves the cascade equations without fluctuations[38] one can still reproduce the average $X_{\max}$ to within a few g/cm$^2$.

### 4.3. Sensitivity of $X_{\max}$ to the $x_F$ distribution

Finally, we analyze which region of the $x_F$-distribution is most important for the mean $X_{\max}$ of an air shower. From the simple argument that forward particles carry most of the energy it should be clear that the high $x_F$ region is important. Our goal here is to quantify this statement somewhat.

Given $dN_n/dx_F$ distributions of secondaries, to study the sensitivity of $X_{\max}$ to various regions of $x_F$ we solve the cascade equations with a modified distribution:

$$\frac{dN_n}{dx_F} \to \frac{dN_n}{dx_F}(1 + \epsilon) \ \text{ for } x_F < x_F^0 \ . \tag{25}$$

That is, we enhance or suppress the spectra at $x_F < x_F^0$ relative to the default reference distributions, depending on the sign of $\epsilon$. At the same time, we suppress or enhance particles at $x_F > x_F^0$ in such a way as to conserve the total energy:

$$\frac{dN_n}{dx_F} \to \frac{dN_n}{dx_F}(1 - \epsilon') \ \text{ for } x_F > x_F^0 \ , \tag{26}$$

with

$$\epsilon' = \epsilon \; \frac{\sum\limits_{n} \int\limits_{0}^{x_F^0} dx_F \; E_n(x_F) \; \frac{dN_n}{dx_F}}{\sum\limits_{n} \int\limits_{x_F^0}^{1} dx_F \; E_n(x_F) \; \frac{dN_n}{dx_F}} \; . \tag{27}$$

Note that the $dN_n/dx_F$ are, of course, energy dependent while we take the $1+\epsilon$ factor in (25) to be constant. Also, we do not modify the inelastic cross section (i.e. the mean free path in the atmosphere), just the $x_F$-distribution of secondaries in an inelastic event. We then solve eqs. (24) to determine the change of $X_{\max}$ relative to that for the reference distributions as a function of both $\epsilon$ and $x_F^0$.
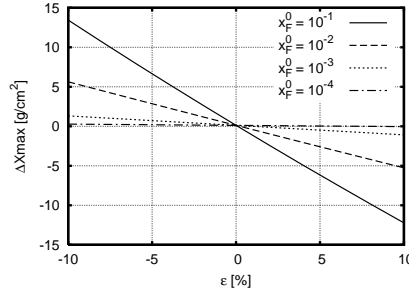


Figure 8.   The shift of $X_{\max}$ as a function of $\epsilon$ for various $x_F^0$. This shows that the shower maximum is sensitive to mainly the forward region, $x_F \gtrsim 10^{-3}$.

The result is shown in Fig. 8, assuming a proton primary with energy $E_0 = 10^{10}$ GeV. The reference $dN_n/dx_F$ distributions were taken from QGSJET01. We observe that $\Delta X_{\max}$ is approximately linear in $\epsilon$. For large $x_F^0$, for example =0.1, there is a significant shift $\Delta X_{\max} \approx 140\epsilon$. For $\epsilon < 0$ we suppress the $x_F < 0.1$ region and, by energy conservation, enhance the large-$x_F$ part; this leads to deeper penetration into the atmosphere, i.e. to larger $X_{\max}$. In turn, *suppression* of forward particle production ($\epsilon > 0$ and $\epsilon' < 0$) leads to decreasing $X_{\max}$.

However, one can also observe that $X_{\max}$ becomes independent of $\epsilon$ for $x_F^0 \lesssim 10^{-3}$. This shows that the small-$x_F$ part of the distribution has no influence on the shower maximum (for fixed cross section). For comparison, we note that a particle produced at mid-rapidity (in a collision with energy $10^{10}$ GeV) with an energy of about the proton mass has $x_F \simeq 10^{-5}$.

24

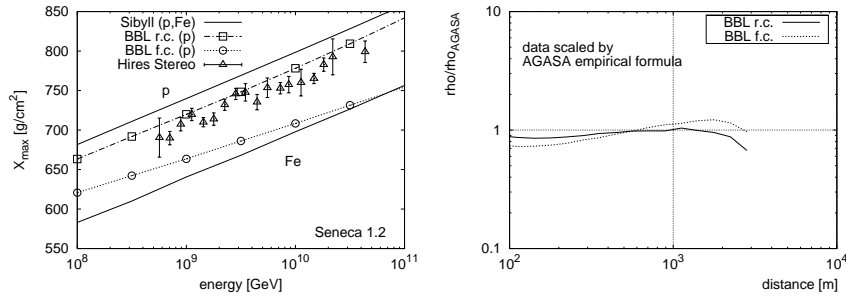## 5. Application of the BBL to air showers



Figure 9.   Left panel: mean $X_{\max}(E_0)$ for $p$ and $Fe$ induced showers from SIBYLL 2.1, and for $p$ primaries with BBL for fixed and running coupling evolution; data are from HIRES[2]; figure from[8]. Right panel: mean lateral distribution function scaled by the LDF found by AGASA.

To apply our interaction model to air showers, we tabulated $dN_n/dE$ distributions of the primary particles appearing in an air shower. We then employ the SENECA[34] model to solve the cascade equations (24). The hadron-air inelastic cross sections are taken as parameterized in SIBYLL 2.1. In Fig. 9 we compare the results for fixed and running coupling evolution to those obtained with the SIBYLL 2.1 model. One notices a huge difference between fixed and running coupling evolution scenarios. The saturation momentum in the former case is so high that forward scattering is very strongly suppressed over a broad range of impact parameters; also, the discrepancy between those evolution scenarios at the highest energies is strongly amplified by subsequent hadronic collisions in the cosmic ray cascade. Consequently, for fixed coupling evolution the shower is absorbed very early in the atmosphere. Hence, if we assume a hadronic primary, then the HIRES[2] data excludes this scenario, since it would require hadrons lighter than protons. This is a novel result as present accelerator data could not rule out such a rapid growth of the gluon density (see e.g.[24,20]); it illustrates the ability of cosmic ray air showers to provide observational constraints on small-$x$ QCD [8].

The running coupling result, on the other hand, is compatible with those data and with a light composition. The results from this model are similar to those from SIBYLL 2.1 or QGSJET01 (for proton primaries) within present theoretical uncertainties. Nevertheless, our results show that the effects discussed here make near-GZK proton-induced air showers look more

similar to nucleus-induced cascades from leading-twist models and so favor a lighter composition near the cutoff.

Lateral distribution functions obtained with both evolution scenarios are shown in the right panel of Fig. 9. The LDFs were computed for the AGASA experiment and include a full detector response simulation of the plastic scintillators. The results are scaled by the empirical formula which describes the data up to highest energies quite well:

$$S(R) = C \left( \frac{R}{R_M} \right)^{-\alpha} \left( 1 + \frac{R}{R_M} \right)^{-(\eta-\alpha)} \left( 1 + \left( \frac{R}{1 \text{ km}} \right)^2 \right)^{-\delta}, \qquad (28)$$

with $\alpha = 1.2$, $\delta = 0.6$, $R_M = 91.6$ m and $\eta = 3.84$ for vertical showers[39]. The parameter $C$ is adjusted using the energy conversion formula (13) from Ref. [39],

$$E = 2.17 \times 10^{17} \ S(600 \text{ m}) \, \text{eV}, \qquad (29)$$

which is valid for the average altitude of the AGASA array, =667 m. The comparison in Fig. 9 shows that the LDF obtained for fixed coupling evolution is much flatter than that for running coupling evolution, which in turn agrees better with the data (notice that in the figure, the theoretical curves are scaled by the data). This is consistent with our finding for $X_{\max}$, as discussed above. When the shower is absorbed earlier in the atmosphere then it spreads out to larger radial distances from the shower axis.

## 6. Conclusion and Outlook

In this paper we pointed out that atmospheric air showers induced by the highest energy cosmic rays are sensitive to QCD interactions at extremely small momentum fractions $x$ where nonlinear effects are expected to play a major role and lead to unitarization of partonic scattering cross sections. In turn, this means that cosmic rays air showers can provide valuable insight and observational constraints for the strong-field regime of QCD. As an example, we have shown that present data on $X_{\max}(E)$ already exclude that the rapid $\sim 1/x^{0.3}$ growth of the saturation boundary (which is compatible with RHIC and HERA data) persists up to GZK cutoff energies[8].

The model used here for quantitative calculations can be improved in many ways, for example by incorporating more advanced estimates for the small-$x$ gluon densities obtained from the approaches of refs[4,5]. From the point of view of learning about cosmic rays from small-$x$ QCD it could be interesting to extend the studies to nucleus-nucleus collisions and to

perform a composition analysis near the cutoff. This might also be relevant for physics well below the cutoff, in the region above the "knee"[40] ($E \simeq 5 \cdot 10^6$ GeV) because for nuclei nonlinearities should set in at lower energies already.

Cosmic ray air showers offer several important advantages over laboratory experiments: first of all, of course, their energies can exceed those of accelerators (even LHC) by far. Second, many properties of extensive air showers are sensitive mainly to the forward region and to transverse momenta about $\langle p_t \rangle$, which means that they probe extremely small $x$ in the target nucleus. Finally, an air shower develops via several subsequent collisions and so any "distortion" of the momentum-space distribution of secondaries from high-density effects is strongly amplified (essentially raised to the power of the number of collisions).

On the other hand, unlike air shower detectors accelerator experiments can control key parameters of the interaction. For example, aside from collision energy and centrality one can also chose various projectiles and targets, from protons over light nuclei up to very massive nuclei such as gold or lead. Central collisions on lead at LHC energy should provide similar gluon densities as those on air at cutoff energies. Hence, fruitful lessons regarding small-$x$ QCD will hopefully emerge from both cosmic ray and accelerator data in the future. We emphasize that crucial data to be obtained at the LHC is not limited to the total proton-proton cross section but includes $x_F$ distributions of secondaries from $p+A$ collisions in both the central and forward regions. The latter would allow us to study the energy degradation mechanism in central collisions, which plays an important role for cosmic ray air showers.

### Acknowledgements

## References

1. S. Yoshida et al., Astropart. Phys. **3**, 105 (1995).
2. P. V. Sokolsky for the HiRes Collaboration, *Prepared for 28th International Cosmic Ray Conference (ICRC 03), Tsukuba, Japan, July 31 – Aug. 7, 2003*, p. 405;
   High Resolution Fly's Eye Collaboration, arXiv:astro-ph/0407622.
3. Auger: www.auger.org
4. G. Altarelli, R. D. Ball and S. Forte, Nucl. Phys. B **674**, 459 (2003).
5. M. Ciafaloni, D. Colferai, G. P. Salam and A. M. Stasto, Phys. Rev. D **68**, 114003 (2003).
6. L. Frankfurt, V. Guzey, M. McDermott and M. Strikman, Phys. Rev. Lett. **87**, 192301 (2001).
7. A. Dumitru, L. Gerland and M. Strikman, Phys. Rev. Lett. **90**, 092301 (2003) [Erratum-ibid. **91**, 259901 (2003)].
8. H. J. Drescher, A. Dumitru and M. Strikman, arXiv:hep-ph/0408073.
9. L. V. Gribov, E. M. Levin and M. G. Ryskin, Phys. Rept. **100**, 1 (1983);
   A. H. Mueller and J. Qiu, Nucl. Phys. B **268**, 427 (1986);
   I. Balitsky, Nucl. Phys. B **463**, 99 (1996);
   J. Jalilian-Marian, A. Kovner, A. Leonidov and H. Weigert, Phys. Rev. D **59**, 034007 (1999) [Erratum-ibid. D **59**, 099903 (1999)];
   E. Iancu, A. Leonidov and L. D. McLerran, Nucl. Phys. A **692**, 583 (2001);
   A. Kovner and U. A. Wiedemann, Phys. Rev. D **66**, 034031 (2002).
10. L. McLerran and R. Venugopalan, Phys. Rev. D **49**, 2233 (1994); ibid. **49**, 3352 (1994);
    Y. V. Kovchegov, ibid. **54**, 5463 (1996); ibid. **55**, 5445 (1997);
11. A. H. Mueller, Nucl. Phys. B **558**, 285 (1999).
12. V. N. Gribov and L. N. Lipatov, Yad. Fiz. **15**, 781 (1972) [Sov. J. Nucl. Phys. **15**, 438 (1972)];
    Yu. L. Dokshitzer, Sov. Phys. JETP **46**, 641 (1977) [Zh. Eksp. Teor. Fiz. **73**, 1216 (1977)];
    G. Altarelli and G. Parisi, Nucl. Phys. B **126**, 298 (1977).
13. A. Dumitru and J. Jalilian-Marian, Phys. Rev. Lett. **89**, 022301 (2002).
14. M. Gyulassy and L. D. McLerran, Phys. Rev. C **56**, 2219 (1997).
15. L. L. Frankfurt and M. I. Strikman, Phys. Rept. **160**, 235 (1988).
16. F. Gelis and A. Peshier, Nucl. Phys. A **697**, 879 (2002);
    F. Gelis and J. Jalilian-Marian, Phys. Rev. D **67**, 074019 (2003).
17. D. Boer and A. Dumitru, Phys. Lett. B **556**, 33 (2003);
18. E. Iancu, K. Itakura and L. McLerran, Nucl. Phys. A **724**, 181 (2003).
19. Y. V. Kovchegov and A. H. Mueller, Nucl. Phys. B **529**, 451 (1998);
    B. Z. Kopeliovich, A. V. Tarasov and A. Schäfer, Phys. Rev. C **59**, 1609 (1999);
    A. Dumitru and L. D. McLerran, Nucl. Phys. A **700**, 492 (2002);
    A. Dumitru and J. Jalilian-Marian, Phys. Lett. B **547**, 15 (2002);
    J. Jalilian-Marian, Y. Nara and R. Venugopalan, Phys. Lett. B **577**, 54 (2003);
    J. P. Blaizot, F. Gelis and R. Venugopalan, Nucl. Phys. A **743**, 13 (2004).

28

20.  D. Kharzeev, E. Levin and L. McLerran, Phys. Lett. B **561**, 93 (2003);
     D. Kharzeev, E. Levin and M. Nardi, Nucl. Phys. A **730**, 448 (2004).
21.  A. Krasnitz and R. Venugopalan, Phys. Rev. Lett. **86**, 1717 (2001);
     A. Krasnitz, Y. Nara and R. Venugopalan, Phys. Rev. Lett. **87**, 192302 (2001).
22.  H. L. Lai *et al.* [CTEQ Collaboration], Eur. Phys. J. C **12**, 375 (2000).
23.  E. Iancu and R. Venugopalan, arXiv:hep-ph/0303204.
24.  K. Golec-Biernat and M. Wusthoff, Phys. Rev. D **59**, 014017 (1999).
25.  D. N. Triantafyllopoulos, Nucl. Phys. B **648**, 293 (2003).
26.  M. Glück, E. Reya and A. Vogt, Z. Phys. C **67**, 433 (1995).
27.  M. Glück, E. Reya and A. Vogt, Z. Phys. C **53**, 651 (1992).
28.  B. Andersson, G. Gustafson, G. Ingelman and T. Sjöstrand, Phys. Rept. **97**,
     31 (1983);
     T. Sjöstrand, P. Eden, C. Friberg, L. Lonnblad, G. Miu, S. Mrenna and E. Nor-
     rbin, Comput. Phys. Commun. **135**, 238 (2001).
29.  R. S. Fletcher, T. K. Gaisser, P. Lipari and T. Stanev, Phys. Rev. D **50**,
     5710 (1994);
     R. Engel, T. K. Gaisser, T. Stanev and P. Lipari, *Prepared for 26th Interna-*
     *tional Cosmic Ray Conference (ICRC 99), Salt Lake City, Utah, 17-25 Aug*
     *1999.*
30.  N. N. Kalmykov, S. S. Ostapchenko and A. I. Pavlov, Nucl. Phys. Proc.
     Suppl. **52B**, 17 (1997).
31.  I. Arsene *et al.* [BRAHMS Collaboration], arXiv:nucl-ex/0401025.
32.  D. Kharzeev, E. Levin and M. Nardi, Nucl. Phys. A **747**, 609 (2005).
33.  T. Gaisser, "Cosmic Rays and Particle Physics", Cambridge University Press
     (1990).
34.  G. Bossard et al., Phys. Rev. **D63**, 054030 (2001);
     H. J. Drescher and G. Farrar, Phys. Rev. **D67**, 116001 (2003).
35.  H. J. Drescher, M. Bleicher, S. Soff and H. Stöcker, Astropart. Phys. **21**, 87
     (2004).
36.  T. K. Gaisser and F. Halzen, Phys. Rev. Lett. **54**, 1754 (1985).
37.  W. R. Nelson, H. Hirayama and D. W. O. Rogers, *The EGS4 Code System*,
     report SLAC-265, Stanford Linear Accelerator Center, 1985.
38.  H. J. Drescher, arXiv:astro-ph/0411144.
39.  M. Takeda et al., Astropart. Phys. **19**, 447 (2003).
40.  K. H. Kampert *et al.* [The KASCADE Collaboration], Nucl. Phys. Proc.
     Suppl. **136**, 273 (2004) [arXiv:astro-ph/0410559].